Electrochimica Acta 176 (2015) 301–310

Contents lists available at ScienceDirect

Electrochimica Acta

journal homepage: www.elsevier.com/locate/electacta

Electrochemical Model for Ionic Liquid Electrolytes in Lithium Batteries

Kisoo Yoo, Anirudh Deshpande, Soumik Banerjee, Prashanta Dutta*

School of Mechanical and Materials Engineering Washington State University, Pullman, Washington 99164-2920, USA

ARTICLE INFO

Article history:
Received 1 May 2015
Received in revised form 26 June 2015
Accepted 1 July 2015
Available online 4 July 2015

Keyword:
Li Battery
Ionic Liquid
Ternary System

ABSTRACT

Room temperature ionic liquids are considered as potential electrolytes for high performance and safe lithium batteries due to their very low vapor pressure and relatively wide electrochemical and thermal stability windows. Unlike organic electrolytes, ionic liquid electrolytes are molten salts at room temperature with dissociated cations and anions. These dissociated ions interfere with the transport of lithium ions in lithium battery. In this study, a mathematical model is developed for transport of ionic components to study the performance of ionic liquid based lithium batteries. The mathematical model is based on a univalent ternary electrolyte frequently encountered in ionic liquid electrolytes of lithium batteries. Owing to the very high concentration of components in ionic liquid, the transport of lithium ions is described by the mutual diffusion phenomena using Maxwell-Stefan diffusivities, which are obtained from atomistic simulation. The model is employed to study a lithium-ion battery where the electrolyte comprises ionic liquid with $mppy^+$ (N-methyl-N-propyl pyrrolidinium) cation and $TFSI^-$ (bis trifluoromethanesulfonyl imide) anion. For a moderate value of reaction rate constant, the electric performance results predicted by the model are in good agreement with experimental data. We also studied the effect of porosity and thickness of separator on the performance of lithium-ion battery using this model. Numerical results indicate that low rate of lithium ion transport causes lithium depleted zone in the porous cathode regions as the porosity decreases or the length of the separator increases. The lithium depleted region is responsible for lower specific capacity in lithium-ion cells. The model presented in this study can be used for design of optimal ionic liquid electrolytes for lithium-ion and lithium-air batteries.

1. Introduction

In the recent decade, developing energy storage devices such as batteries with improved specific energy and power density has come into the spotlight with the ever-growing societal demand for stable energy supply. Among the myriad energy-storage technologies, rechargeable lithium ion batteries are widely used as energy sources for a range of portable electronic devices because of their relatively high energy storage capabilities. However, even when fully developed the highest energy storage achieved by a state-of-the-art lithium-ion battery is too low to meet current demands in the automotive industry such as in electric vehicles and hybrid electric vehicles. One solution to this problem is to develop high voltage battery with new cathode materials. For instance, Hassoun et al. [1] reported that cell voltage can be improved more than 30% by replacing conventional lithium manganese spinel with lithium nickel manganese oxide ($LiNi_{0.5}Mn_{1.5}O_4$). Similar studies have resulted in high cell voltage (> 4 V) with lithium cobalt oxide ($LiCoO_2$) [2], lithium nicklate ($LiNiO_2$) [3] and lithium manganite ($LiMn_2O_4$) [4] cathode materials. However, long term cyclic performances of these high voltage batteries were unsatisfactory with conventional organic liquid based electrolytes due to large operating electric potential range. The high voltage generated by such cathode materials ($LiMn_2O_4$) dissociates widely used organic electrolytes such as propylene carbonate and diethoxyethane [4,5]. Electrolyte oxidation leads to chemical deposition on an electrode surface and develops insulating layer resulting in irreversible losses in capacity [6]. Thus, it is essential to select a suitable electrolyte with wide electrochemical window for the development of high voltage lithium ion battery. To satisfy this need, ionic liquids are very appealing as electrolytes due to their high electrochemical stability [7], extremely low vapor pressure, ultra high resistance to oxidation and reduction, and tunable viscosity and electrochemical properties [8]. Much of this flexibility arises because their physical and chemical properties can be customized over a wide range through selection and chemical modification of their cation and anion [9].

* Corresponding author. Tel.: +1 (509)335-7989; fax: +1 (509) 335-4662.
E-mail address: dutta@mail.wsu.edu (P. Dutta).

http://dx.doi.org/10.1016/j.electacta.2015.07.003
0013-4686/

In recent years, several lithium-ion batteries have been tested using ionic liquids and some experimental works have demonstrated the feasibility of ionic liquid electrolytes in lithium battery at low load current density [10–14]. However, the electrical performance of lithium batteries with ionic liquid electrolytes is inferior to that with organic electrolytes, especially at high load current density. One reason for lower battery performance might be due to lower mobility of lithium ions in ionic liquid electrolytes. Thus, understanding transport mechanism of various ions in ionic liquid electrolyte might provide valuable insights for electrical performance of next generation lithium batteries.

The transport of lithium ions in organic electrolytes is studied extensively to predict the performance of lithium batteries. In a seminal study, Newman et al. [15] developed continuum based electrochemical model to predict the transport of lithium ions in concentrated binary solutions [15–17]. The same group also presented model to take care of porous electrode media in lithium batteries [18,19]. Wang et al. [20] presented a multiscale model to study both fuel cell and batteries, where the concentration of intercalated lithium is estimated using a second order polynomial. Later, Subramanian et al. [21] obtained a close form analytic solution for lithium intercalation into the microparticle considering a spherical shape particle. However, these models cannot be used to predict the lithium ion transport in ionic liquid electrolytes since they are developed for binary electrolytes, where there is only one anion and one cation (see Table 1). To understand the electrical performance in ionic liquid based ternary systems, we developed a mathematical model. This model is employed to study the performance of a lithium-ion battery with ionic liquid electrolyte.

2. Theory

2.1. Ternary System

Room temperature ionic liquid (RTIL) solely consists of ions such as $mppy^+$ and $TFSI^-$. Thus, suitable Li-X (Li-TFSI) salt should be added into RTIL since ions of RTIL are not electroactive [22]. Typically, in an RTIL based electrolyte, all species are totally ionized and the electrolyte consists of two cations and one anion, for instance $mppy^+$, Li^+, $TFSI^-$. In this ternary system, all ions strongly interact with each other. For example, $TFSI^-$ has a tendency to form a cluster around lithium ions, which restricts the movement of lithium ions in ionic liquid electrolyte (see Fig. 1)[23]. Therefore, species transport model [24] (Nernst-Planck equation) developed for a dilute solution is no more applicable in ionic liquid systems since in dilute solution theory there is no interaction between ions. Also, mass conservation equations developed for concentrated binary solution [15] cannot be applied for ionic liquid based ternary electrolytes. However, by considering the mutual diffusion of interacting ions [25], the contribution of ionic interaction can be taken into account in species transport equation.

Maxwell-Stefan equation describes the mutual diffusion for a multi-component system as

$$-\nabla\mu_i = \frac{RT}{C_T}\sum_j\left[\frac{C_j}{D_{ij}}\left(V_i - V_j\right)\right] \tag{1}$$

where D_{ij} is Maxwell-Stefan diffusivity between i and j species, V_i is the velocity of species i, C_j and C_T are concentration of species j and total species concentration, respectively. In an electrochemical cell, the bulk fluid velocity is negligible. Thus, V_i is the velocity of species i due to electrochemical potential only. The electrochemical potential (μ) consists of electric (Φ) and chemical (μ^{chem}) potential expressed as

$$\mu = zF\Phi + \mu^{chem} = zF\Phi + RT\ln(f\cdot C) \tag{2}$$

where R,T, f, and C are gas constant, temperature, chemical activity coefficient and concentration. For isothermal conditions, the gradient of electrochemical potential for a species i is given as

$$\nabla\mu_i = z_iF\nabla\Phi + RT\left(\frac{\nabla f_i}{f_i} + \frac{\nabla C_i}{C_i}\right) \tag{3}$$

Equating Eqs. (1) and (3), one can find relationship among species concentration, activity coefficient and electrochemical velocity as

$$-\frac{RT}{C_T}\sum_j\left[\frac{C_j}{D_{ij}}\left(V_i - V_j\right)\right] = z_iF\nabla\Phi + RT\left(\frac{\nabla f_i}{f_i} + \frac{\nabla C_i}{C_i}\right) \tag{4}$$

The numerical solution of this nonlinear coupled system is very challenging. Here we present a simplified system of equations for electrochemical velocity using some reasonable assumptions such as electroneutrality condition, univalent electrolyte, and mass conservation.

2.1.1. Electroneutrality and Total Species Concentration

For ternary systems, the electroneutrality equation can be expressed as:

Table 1
Comparison between organic liquid based binary electrolyte and ionic liquid based ternary system.

Solvent	Salt	Electrolyte	Ions	System
Organic (propylene carbonate)	$LiPF_6$	Organic Electrolyte	Li^+, $PF6^-$	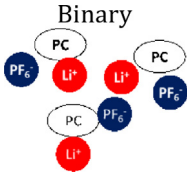
Ionic Liquid (mppy-TFSI)	LiTFSI	Ionic Liquid Electrolyte	Li^+, $mppy^+$, $TFSI^-$	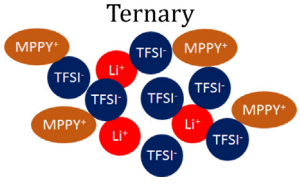

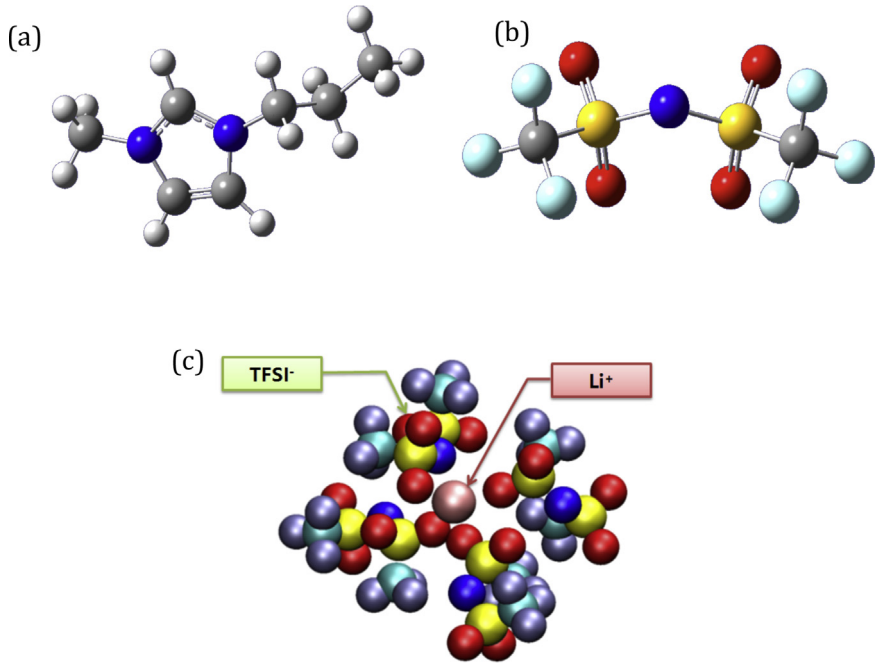

Fig. 1. Molecular structures of (a) mppy$^+$(*N*-methyl-*N*-propyl pyrrolidinium) and (b) TFSI$^-$(bis trifluoromethanesulfonyl imide). (c) Formation of cluster due to coordination of Li^+ with $TFSI^-$ anions in an isotropic and homogeneous liquid.

$$\sum_i z_i C_i = z_1 C_1 + z_2 C_2 + z_3 C_3 = 0 \tag{5}$$

where subscripts 1, 2 and 3 denote 1: Li^+, 2: mppy$^+$, 3: $TFSI^-$, respectively. Using electroneutrality condition (Eq. (5)) and total concentration (C_T) of all components,

$$C_1 + C_2 + C_3 = C_T \tag{6}$$

one can find following simplified relationships

$$C_1 = \frac{z_3}{z_3 - z_1} C_T - \frac{z_3 - z_2}{z_3 - z_1} C_2 \tag{7}$$

$$C_3 = \frac{z_1}{z_1 - z_3} C_T - \frac{z_1 - z_2}{z_1 - z_3} C_2 \tag{8}$$

Here it is assumed that during discharge lithium ion produced at the anode side is consumed at the cathode (vice versa for charge) to keep the total concentration of ionic species to be constant. Thus, Eq. (8) indicates that the concentration of anion is constant in a univalent ternary system ($Z_1 = Z_2 = Z$ and $Z_3 = -Z$). This constant concentration of anion will result in zero net velocity for anions ($V_3 = 0$) throughout the computational domain, which will simplify the model for ternary system significantly.

2.1.2. Ionic Strength and Activity Coefficient

In concentrated solution, like ionic liquid with salt, the activity coefficient is a function of ionic strength *I*. For a ternary electrolyte with completely dissociated ionic liquid and lithium salt, the ionic strength can be found as

$$I = \frac{1}{2}(C_1 + C_2 + C_3) = \frac{1}{2} C_T \tag{9}$$

Since the ionic strength is a constant in a ternary ionic liquid, the gradient of activity coefficient can be eliminated from Eq. (4), and the Maxwell-Stefan equations can be modified as.

$$-RT\frac{\nabla C_1}{C_1} - zF\nabla\Phi = \frac{RT}{C_T}\left[\frac{C_2}{D_{12}}\left(V_1 - V_2\right) + \frac{C_3}{D_{13}} V_1\right] \tag{10a}$$

$$-RT\frac{\nabla C_2}{C_2} - zF\nabla\Phi = \frac{RT}{C_T}\left[\frac{C_1}{D_{12}}\left(V_2 - V_1\right) + \frac{C_3}{D_{23}} V_2\right] \tag{10b}$$

$$zF\nabla\Phi = \frac{RT}{C_T}\left[-\frac{C_1}{D_{13}} V_1 - \frac{C_2}{D_{23}} V_2\right] \tag{10c}$$

2.2. Mathematical Model

2.2.1. Transport Equation for Li ion in Ternary System

From the general mass conservation equation, lithium ion concentration can be formulated as

$$\frac{\partial C_1}{\partial t} + \nabla \cdot \left(N_1\right) = S_1 \tag{11}$$

where N_1 is the flux of lithium ions due to advection, diffusion and electromigration, and S_1 is source or sink term due to lithium oxidation or reduction. As mentioned earlier, in a battery, the bulk velocity due to fluid motion is generally negligible, and the lithium flux can be obtained as

$$N_1 = C_1 V_1 \tag{12}$$

where V_1 is the lithium ion velocity due to diffusion and electromigration. Using equations (10a) and (10c), one can find the flux of lithium ion as

$$C_1 V_1 = -\frac{C_T D_{12} D_{23}}{C_1 D_{23} + C_2 D_{13} + C_3 D_{12}} \nabla C_1 - \left(1 + \frac{D_{23}}{D_{12}}\right) \frac{C_T D_{12} D_{23}}{C_1 D_{23} + C_2 D_{13} + C_3 D_{12}} \frac{zF\nabla\Phi}{RT} C_1 \tag{13}$$

Finally, using Eqs. (7), (8), (10) and (13), we can obtain a transport equation for lithium ions as

$$\frac{\partial C_1}{\partial t} - \nabla \cdot \left(\tilde{D}_1 \nabla C_1 + z\tilde{\omega}_1 \nabla \Phi C\right) = S_1 \tag{14}$$

where $\tilde{D}_1$ and $\tilde{\omega}_1$ are apparent diffusivity and mobility for lithium ion in ionic liquid electrolyte. The apparent diffusivity and mobility can be obtained from Maxwell-Stefan diffusivities (D_{12}, D_{23}, D_{13}) and mole fraction of lithium ions (χ_1) as

$$\tilde{D}_1 = \frac{2D_{12}D_{23}}{D_{12} + D_{13} + 2(D_{23} - D_{13})\chi_1} \tag{15}$$

$$\tilde{\omega}_1 = \left(1 + \frac{D_{23}}{D_{12}}\right)\frac{\tilde{D}_1 F}{RT} \tag{16}$$

The general format of Eq. (14) is same as the Nernst-Planck equation used in dilute electrolyte. However, for ionic liquid based ternary system, one has to use the apparent diffusivity and apparent mobility instead of self diffusivity and absolute mobility. The transport equation for lithium ion (Eq. (14)) is highly nonlinear as both apparent diffusivity and mobility are a function of lithium ion concentration. Thus, it can only be solved using a numerical method.

2.2.2. Liquid Phase Electric Potential in Ternary System

Governing equation for electric potential in the electrolyte can be obtained from charge conservation equation as

$$\nabla \cdot i_l = a_{SP} j_c \tag{17}$$

where i_l and j_c are current density and transfer current density, and a_{SP} is the specific area of cathode material. In a ternary ionic liquid electrolyte system, the current produced by the movement of ions can be expressed as

$$i_l = zF\left(C_1 V_1 + C_2 V_2 - C_3 V_3\right) \tag{18}$$

Using Eqs. (10c) and (13) and setting $\vec{V}_3 = 0$, the current density can be rewritten as

$$i_l = -C_T D_{23} z^2 F\left(\frac{D_{13}/D_{23} - 1}{D_{13}}\tilde{\omega}\chi_1 + \frac{F}{RT}\right)\nabla\Phi_l - \frac{F(D_{13} - D_{23})}{D_{13}}\tilde{D}\nabla C_1 \tag{19}$$

If we define the ionic conductivity as

$$\lambda = C_T D_{23} z^2 F\left(\frac{D_{13}/D_{23} - 1}{D_{13}}\tilde{\omega}\chi_1 + \frac{F}{RT}\right) \tag{20}$$

the charge conservation equation can be expressed as

$$\nabla \cdot \left[\lambda \nabla \Phi_l\right] = -a_{SP} j_c - \nabla \cdot \left[\frac{F(D_{13} - D_{23})}{D_{13}}\tilde{D}\nabla C_1\right] \tag{21}$$

2.2.3. Model Equations for Ionic Liquid based Li-ion Battery

The transport equations developed in the previous section are only valid for a continuous liquid electrolyte medium. However, the separator and cathode regions of a lithium ion battery contain both solid and liquid. Thus, we need to modify the transport equations developed in the previous section for porous materials. Using Bruggeman correlation [26], the governing equation for lithium ion transport can be expressed as

$$\frac{\partial(\varepsilon C_{Li^+})}{\partial t} - \nabla \cdot \left[\varepsilon^{1.5}\tilde{D}_{Li^+}\nabla C_{Li^+} + z\tilde{\omega}_{Li^+}\nabla\Phi_l(\varepsilon C_{Li^+})\right] = \frac{a_{sp} j_c}{F} \tag{22}$$

where j_c is the local current density. Similarly, the governing equation for the solid and liquid phase electric potential can be modified for porous media as

$$\nabla \cdot (\lambda \varepsilon^{1.5}\nabla\Phi_l) = -a_{sp} j_c - \nabla \cdot \left[\frac{F(D_{13} - D_{23})}{D_{13}}\varepsilon^{1.5}\tilde{D}\nabla C_1\right] \tag{23}$$

$$\nabla \cdot \left[\sigma(1-\varepsilon)^{1.5}\nabla\Phi_s\right] = a_{sp} j_c \tag{24}$$

where σ is electrical conductivity.

In a lithium-ion battery, the local transfer current density at the reaction sites can be calculated using the Butler-Volmer Equation as [16,27,28]

Anode:

$$j_a = i_0\left\{\exp\left[\frac{\beta nF}{RT}\eta_a\right] - \exp\left[-\frac{(1-\beta)nF}{RT}\eta_a\right]\right\} \tag{25}$$

Cathode:

$$j_c = Fk_0\sqrt{C_{Li^+}\left(C_S^{\max} - C_S^{surf}\right)C_S^{surf}}\left[\exp\left(\frac{\beta nF}{RT}\eta_c\right) - \exp\left(-\frac{(1-\beta)nF}{RT}\eta_c\right)\right] \tag{26}$$

where i_0 is the current density coefficient, β, F and k_0 are the symmetric coefficient, Faraday constant and reaction constant, and $C_s^{\max}$ and C_s^{surf} are maximum lithium concentration in cathode material and surface lithium concentration in the active cathode material. The surface overpotential can be expressed as.

$$\eta = \Phi_s - \Phi_l - E \tag{27}$$

where Φ_s and Φ_l are solid and liquid phase electric potential. For a lithium metal anode, the open circuit potential (E) is a constant at the anode side since the reactant (lithium) concentration does not change. However, the open circuit potential varies at the cathode side depending on the amount of intercalation into the cathode material. Thus, the cathode side open circuit potential is a function of electrode utilization (n), which can be expressed as

$$n = \frac{C_s^{avg}}{C_{CoO_2}} \tag{28}$$

where C_{CoO_2} is the volume average concentration of cobalt oxide and C_s^{avg} is the average concentration of intercalated lithium into the cathode particle, which can be calculated from mass conservation equation as

$$\frac{dC_s^{avg}}{dt} = -\frac{a_{sp} j_c}{F} \tag{29}$$

The surface lithium concentration is related to the average concentration of intercalated lithium by

$$C_s^{suf} = C_s^{avg} - \frac{l_s\, a_{sp} j_c}{D_s\ F} \tag{30}$$

where l_s and D_s are diffusion length and diffusivity of intercalated Li into cathode material, respectively.

3. Properties of Ionic Liquid Electrolyte

In the continuum model analysis, Maxwell-Stefan diffusivities are properties of multi-component system and should be given. Unfortunately, it is difficult to obtain Maxwell-Stefan diffusivities from experiment. But molecular dynamics (MD) simulations can be applied to find these diffusivities [29]. In this study, we used MD simulations to evaluate Maxwell-Stefan diffusivities as well as electrochemical properties of the chemical species in the ternary system consisting of $mppy^+$ $TFSI^-$ ionic liquid (IL) doped with Li^+TFSI^-. Ab initio charge calculations were performed on a cation/anion pair with the second-order Moller–Plesset (MP2) perturbation theory using the 6-31G (d) basis set [30,31] to obtain the

partial atomic charges. As described in our previous work [23], the charges were reduced to account for polarization effects. We used the software LAMMPS [32] for all classical MD simulations. All atomic interactions were described using the optimized potentials for liquid simulations (OPLS) force field [33]. For the doped solution (IL with Li^+TFSI^-), a mixture of 0.25 mole fraction Li^+TFSI^- with 0.75 mole fraction $mppy^+$ $TFSI^-$ was simulated.

An *NPT* ensemble, where the number of particles (N), pressure (P), and temperature (T) are fixed, was used to equilibrate the system at atmospheric pressure and temperature of 303 K. A Nose'–Hoover barostat [34] and thermostat [35] were utilized to control the pressure and temperature, respectively. Production runs of *NVT* ensembles, where the volume (V) is fixed, were carried out for at least 80 ns. The equations of motion were integrated with a time step of 1 fs. The cutoff distances for Columbic interactions and van der Waals were 1.5 nm. Long range electrostatic interactions were computed using the particle–particle–particle mesh (PPPM) method [36,37].

The Maxwell-Stefan diffusivities are obtained from Onsager coefficients (μ) [29,38], which is calculated from molecular dynamics simulations, using the following equation:

$$\mu_{ab} = \frac{1}{6}\lim_{n\to\infty}\frac{1}{N}\cdot\frac{1}{n\cdot\Delta t}\left\langle\left\{\sum_{i=1}^{N_a}\left[r_{i,a}(t+n\cdot\Delta t)-r_{i,a}(t)\right]\right\}\left\{\sum_{j=1}^{N_b}\left[r_{j,b}(t+n\cdot\Delta t)-r_{j,b}(t)\right]\right\}\right\rangle \tag{31}$$

Here, a and b are the types of ions, N is the total number of ions, $r_{i,a}$ denotes the position of i^{th} ion of type a at time t, Δt is the simulation time-step, and n is the number of time-steps. $\langle\rangle$ denotes the ensemble average computed over n. Here, the matrix [μ] is symmetric.

In a ternary system, Onsager coefficients μ_{ab} are used to evaluate the matrix 'γ'. The matrix 'γ' is defined as:

$$\gamma = \begin{bmatrix}\gamma_{11} & \gamma_{12}\\ \gamma_{21} & \gamma_{22}\end{bmatrix} \tag{32}$$

The elements of γ are defined as:

$$\gamma_{11} = (1-\chi_1)\left(\frac{\mu_{11}}{\chi_1}-\frac{\mu_{13}}{\chi_3}\right) - \chi_1\left(\frac{\mu_{21}}{\chi_1}-\frac{\mu_{23}}{\chi_3}+\frac{\mu_{31}}{\chi_1}-\frac{\mu_{33}}{\chi_3}\right) \tag{33a}$$

$$\gamma_{12} = (1-\chi_1)\left(\frac{\mu_{12}}{\chi_2}-\frac{\mu_{13}}{\chi_3}\right) - \chi_1\left(\frac{\mu_{22}}{\chi_2}-\frac{\mu_{23}}{\chi_3}+\frac{\mu_{32}}{\chi_2}-\frac{\mu_{33}}{\chi_3}\right) \tag{33b}$$

$$\gamma_{21} = (1-\chi_2)\left(\frac{\mu_{21}}{\chi_1}-\frac{\mu_{23}}{\chi_3}\right) - x_2\left(\frac{\mu_{11}}{\chi_1}-\frac{\mu_{13}}{\chi_3}+\frac{\mu_{31}}{\chi_1}-\frac{\mu_{33}}{\chi_3}\right) \tag{33c}$$

$$\gamma_{22} = (1-\chi_2)\left(\frac{\mu_{22}}{\chi_2}-\frac{\mu_{23}}{\chi_3}\right) - \chi_2\left(\frac{\mu_{12}}{\chi_2}-\frac{\mu_{13}}{\chi_3}+\frac{\mu_{32}}{\chi_2}-\frac{\mu_{33}}{\chi_3}\right) \tag{33-d}$$

Here, '1′ refers to Li^+, '2′ refers to $mppy^+$ and '3′ refers to $TFSI^-$. The matrix γ is inverted to obtain Matrix β

$$[\gamma]^{-1} = [\beta] \tag{34}$$

and the elements of matrix β can be used to obtain Maxwell-Stefan diffusivities as

$$D_{12} = \frac{1}{\beta_{11}-\frac{\chi_1+\chi_3}{\chi_1}\beta_{12}} \tag{35a}$$

$$D_{13} = \frac{1}{\beta_{11}+\frac{\chi_2}{\chi_1}\beta_{12}} \tag{35b}$$

$$D_{23} = \frac{1}{\beta_{22}+\frac{\chi_1}{\chi_2}\beta_{21}} \tag{35c}$$

Solving Eqs. (31) through (35), one can obtain the Maxwell-Stefan diffusivities for various components in the system with Li^+TFSI^- - $mppy^+TFSI^-$.

4. Numerical Method

We developed an in house numerical model to solve the coupled mass and charge conservation equations to obtain lithium ion concentration as well as electric potential in both solid and liquid phase. In this study, we assumed a lithium foil anode, and the anode reaction interface does not change with time. In other words, the volume change phenomena as well as dendrite formation at solid electrolyte interface (SEI) is not considered. Although microscopic structure change is very common at the anode reaction interface, this numerical model is intended to capture macroscopic phenomena with appropriate reaction rate constants.

Governing equations for liquid phase potential and lithium ions are solved between anode reaction surface and the right end of the cathode (see Fig. 2). The solid phase electric potential equation is

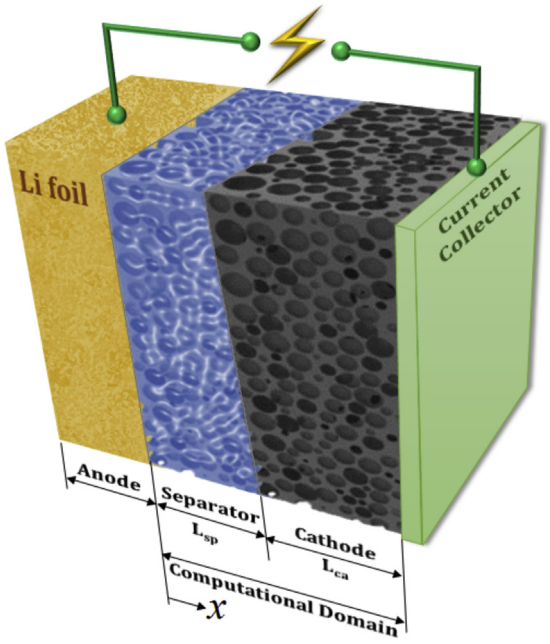

Fig. 2. Schematic of a lithium-ion battery. The computational domain ranges from the interface of anode and separator ($x=0$) to the end of the cathode ($x=L_{sp}+L_{ca}$.

Table 2
Boundary conditions for the governing equations

	Anode reaction surface	Cathode left end	Cathode right end
Lithium ion concentration (C_{Li^+})	$-D_{Li,eff}\frac{\partial C_{Li^+}}{\partial x} = \frac{I_{load}}{F}$	–	$\frac{\partial C_{Li^+}}{\partial x} = 0$
Liquid phase electric potential (ϕ_l)	$-\lambda_{eff}\frac{\partial \phi_l}{\partial x} = I_{load}$	–	$\frac{\partial \phi_l}{\partial x} = 0$
Solid phase electric potential (ϕ_s)	–	$\frac{\partial \phi_s}{\partial x} = 0$	$-\sigma_{eff}\frac{\partial \phi_s}{\partial x} = I_{load}$

Table 3
Maxwell-Stefan diffusivities at 303 K obtained from molecular dynamics simulations.

D_{12}	8.43×10^{-13}	$[m^2/sec]$
D_{13}	4.12×10^{-12}	
D_{23}	6.91×10^{-12}	

*Index 1: Li^+, 2: $mppy^+$, 3: $TFSI^-$

solved only within the porous cathode region. The source term for the lithium ion transport (Eq. (22)) is obtained from Butler-Volmer Eq. (26), where the lithium ion intercalated into the cathode materials (C_s^{avg}) is found from the solution of Eq. (29).

The governing partial differential equations (Eqs. (22), (23) and (24)) are discretized using finite volume method [39] for boundary conditions shown in Table 2. For unsteady term, a first order implicit scheme is used, while for electromigration and diffusion terms second order central differencing technique is used. The discretized algebraic equations are solved with Thomas algorithm until converged results are obtained for C_{Li^+}, Φ_s and Φ_l. The convergence tolerance is set at 10^{-5} for all three variables. The Runge-Kutta fourth order scheme is used to calculate C_s^{avg} from Eq. (29).

5. Results and Discussion

5.1. Maxwell-Stefan Diffusivities

The values of the Maxwell-Stefan diffusivities obtained from the atomistic simulations are given in the Table 3. We observe that the Maxwell-Stefan diffusivity between Li^+- $mppy^+$ is the lowest. This is interpreted in light of the positive charges on both the species and the repulsion between Li^+ and $mppy^+$, which results in relatively diminished diffusion of Li^+ into $mppy^+$. The Maxwell-Stefan diffusivities are relatively higher for Li^+- $TFSI^-$ and $mppy^+$-$TFSI^-$ because of the opposite charges on the ion-pairs, which implicitly accounts for greater attraction between the ion-pairs, thus resulting in increased diffusion into each other. The diffusion between Li^+- $TFSI^-$ is, however, low compared to that of $mppy^+$-$TFSI^-$ because of the increased coordination between Li^+ and $TFSI^-$, which tends to form charged clusters. The smaller Li^+ is surrounded by multiple large $TFSI^-$ ions. This reduces the mobility of the two species and hence the Maxwell-Stefan diffusivity. In case of $mppy^+$- $TFSI^-$, because of similar sizes, there is no cluster formation. Also, because of their large sizes, the surface charge densities of $mppy^+$ and $TFSI^-$ are low. This results in high mutual diffusion between the two species. The high Maxwell-Stefan diffusivity in $mppy^+$-$TFSI^-$ can ultimately be attributed to the high

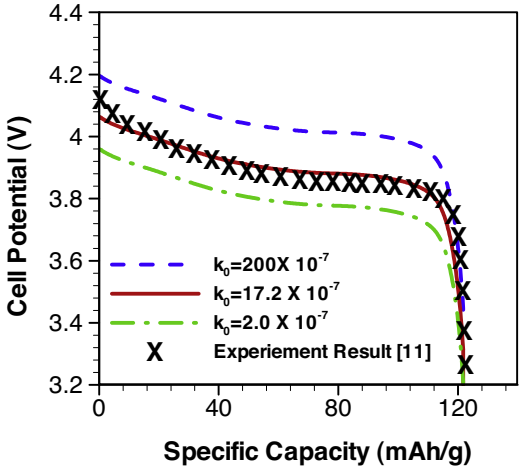

Fig. 3. Predicted cell performance for different value of cathode reaction rate constants for an ionic liquid (0.25 mole fraction of Li^+TFSI^- doped with 0.75 mole fraction $mppy^+$ $TFSI^-$) based lithium ion battery. Experimental results, obtained from the work of Sakaebe and Matsumoto [11] for an identical system, are used for selection of appropriate cathode reaction rate constants. The porosity for cathode and separator are 0.3 and 0.4 respectively based on the work presented in [11], while the cathode and separator thickness are 40 μm and 15 μm respectively. Maxwell-Stefan diffusivities of species are obtained from the molecular simulations to calculate mobility and ionic conductivity for the continuum model. The open circuit potential (E) at the anode side was set as reference, while at the cathodic side it is obtained from the experimental work [42] as a function of electrode utilization (n). The initial value of n is set as 0.58.

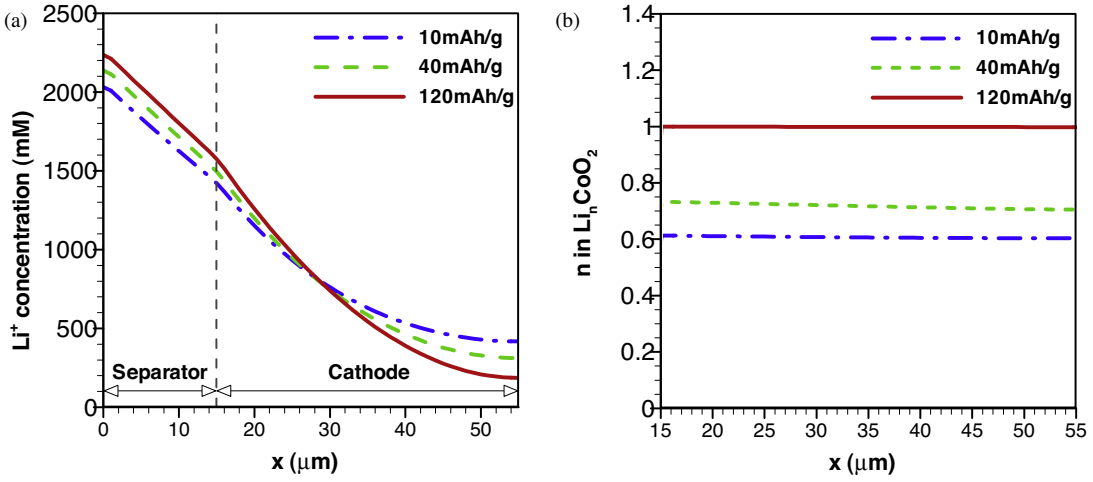

Fig. 4. (a) Lithium ion concentration distribution in the separator and cathode regions. (b) Changes in the cathode utilization with specific capacity. All other simulation conditions are same as in Fig. 3.

cation-anion interaction in ionic liquids [29], as compared to the other species added to the ionic liquid.

5.2. Validation of Proposed Continuum Model for Ternary System

The proposed model is validated by comparing our numerical results with the experimental work of Sakaebe and Matsumoto [11], whereby they have measured the performance of lithium-ion batteries for a number of ionic liquid electrolytes using lithium metal foil and porous $LiCoO_2$ as anode and cathode materials respectively. We specifically chose the mppy^{+}TFSI^{-} doped with Li-TFSI salt (3:1) as ionic liquid electrolyte due to the availability of Maxwell-Stefan diffusivities from molecular simulation. Even though Maxwell-Stefan diffusivities can be calculated using MD, the cathode reaction constant (k_0) affecting kinetic resistance is still unknown for our system. Fig. 3 shows the parametric studies to find the appropriate k_0 for our system. Numerical results predict poor operating cell potential for the low reaction constant ($k_0 = 2 \times 10^{-7}$) case as lower rate will provide higher kinetic resistance at the reaction surface. On the other hand, the operating cell potential will be enhanced with higher reaction constant ($k_0 = 200 \times 10^{-7}$) due to less kinetic loss. For a moderate cathode reaction constant of 17.2×10^{-7} m$^{5/2}$/mole$^{1/2}$-sec, our numerical results show very good agreement with the experimental results for an identical system. Thus, for the rest of the paper, we used this value of cathode reaction constant.

Fig. 4(a) shows the lithium ion concentration distribution in the separator and porous cathodic side for various specific capacities. The results illustrate how lithium concentration changes with time during discharge since we maintained a constant load current

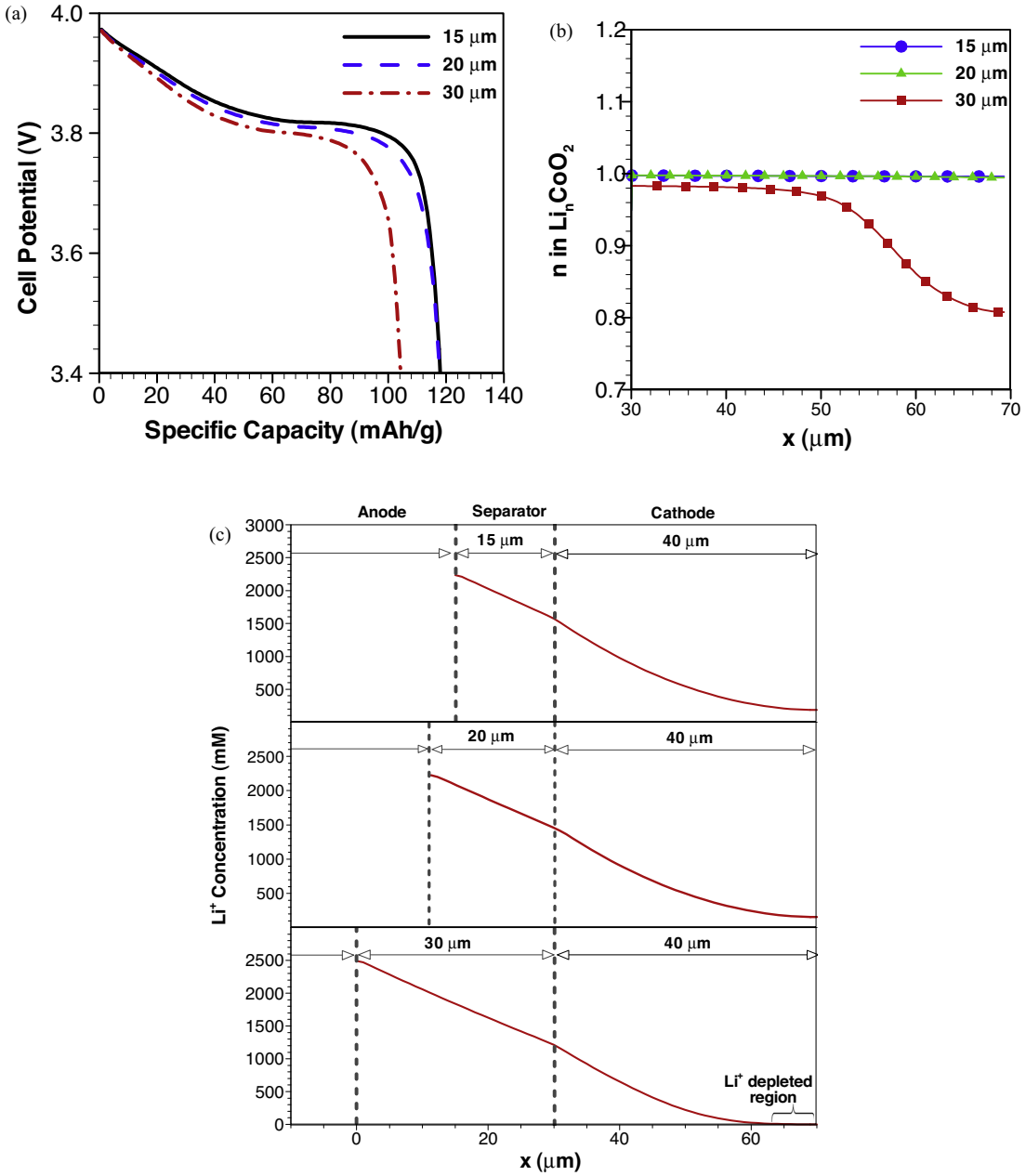

Fig. 5. Effect of separator thickness on the (a) electric performance of battery, (b) cathode material utilization (n) at the fully discharged state, and (c) lithium ion concentration distribution at the fully discharged state. Here all geometric and design parameters are identical for all cases, except the separator thickness. All other simulation conditions are the same as in Fig. 3.

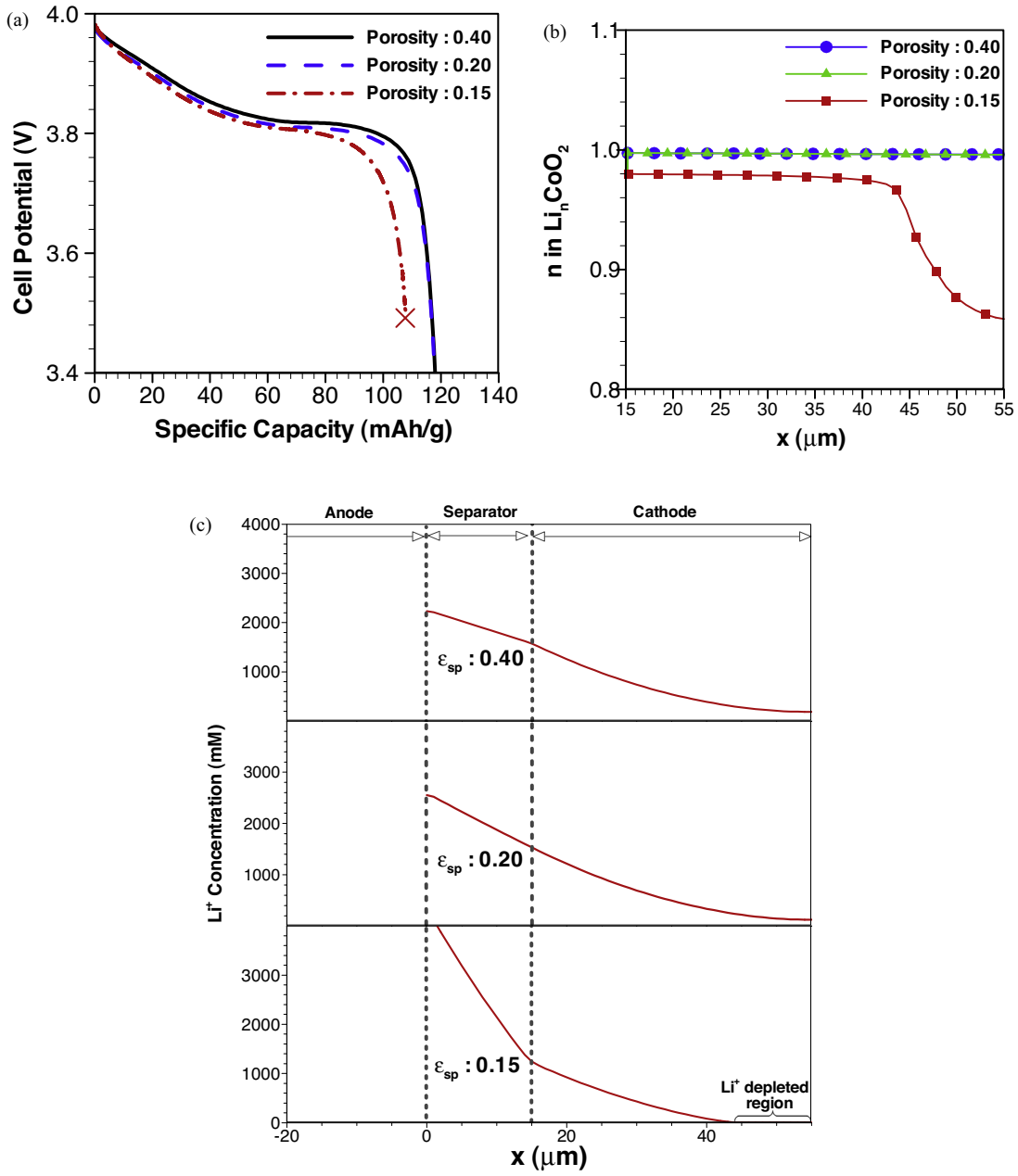

Fig. 6. Effect of separator porosity on the (a) electric performance of a lithium-ion battery, (b) cathode material utilization (n) at the fully discharged state, and (c) lithium ion concentration distribution at the fully discharged state. All other simulation conditions are same as in Fig. 3.

density in our study. As time progresses, the concentration of lithium ion increases in the vicinity of anode as more lithium ions get dissolved in the solution due to lithium oxidation, while it decreases in the cathodic side due to reduction reaction at the cathode sites. The electrode utilization constant (n) keeps on increasing in the cathode side as shown in Fig. 4(b). At the end of the discharge phase, the utilization approaches to unity indicating that there is no site available for further intercalation of lithium ions. These numerical results show that the proposed model not only can validate the experimental electric performance, but can be used to predict the discharge characteristics at various times.

5.3. Study of Lithium Ion Battery using Ionic Liquid Electrolyte

Recently Sahapastsombut *et al.* [40] used Damköhler number to map out the important parameters affecting the performance of a lithium-air battery. They identified that in lithium-air battery with organic electrolyte, the oxygen transport limitation is the crucial factor for poor performance. They also found that the performance of lithium-air battery is limited if the Damköhler number is greater than unity. However, in lithium-ion battery, the cell performance is dependent on the effective mobility of lithium ions as well as the availability of reduction reaction sites in porous cathode. Following the work of Sahapastsombut *et al.*, *the* Damköhler number, a ratio of reaction rate to diffusive mass transfer rate, is defined for a lithium-ion battery as

$$D_a = \frac{i_{load}/F}{\tilde{D}_{Li,eff} C_{Li^+}/(L_{sp} + L_{ca})} \tag{36}$$

This aforementioned equation suggests that the performance will be dependent on parameters such as separator thickness (L_{sp}),

cathode thickness (L_{ca}), load current density (i_{load}), and effective diffusivity. In following section, we studied how these parameters individually affect the performance of a lithium-ion battery working with a model ionic liquid (mppy^{+}TFSI^{-} doped with Li-TFSI salt).

5.3.1. Effect of Separator

In a lithium ion battery, a separator is placed between anode and cathode to prevent physical contact between anode and cathode reaction sites. Ideally an ultra-thin separator with high porosity is desired, but due to technical challenges it is not always possible to make them both very thin and highly porous [41]. For instance, highly porous membranes tend to shrink, while very thin separators cannot withstand the tension of the winding operation during battery operation. To study the effect of separator thickness on the performance of lithium-ion battery, we considered three different separator thicknesses: 15, 20 and 30 microns.

Electric performance of lithium ion battery is presented in Fig. 5(a) for a 40 micron thick cathode. Our numerical results reveal that performance of the battery remains almost unaffected if the separator thickness increases from 15 microns to 20 microns. However, a significant difference in specific capacity is observed once the thickness increased to 30 microns. The lower specific capacity in thicker separator can be explained from the low utilization of active cathode material. As seen from Fig. 5(b), the electrode utilization (n) was very low at the distal end of the cathode. The main reason for low electrode utilization for a thicker separator is primarily due to the lithium depleted region at the distal side of the cathode. Fig. 5(c) presents lithium ion concentration during final stage of discharge for all three different separators. In all three cases, the initial concentration of lithium ions was 1 M. As expected, the lithium ion concentration increases at the anodic side and decreases at the cathodic side due to oxidation and reduction reactions. However, as shown in Fig. 5(c), no lithium ions are available for intercalation at the distal side of the cathode for 30 microns thick separator. This lithium depleted region grows as the discharge continues, and it will worsen for a thicker separator. This result suggests that there is an optimum value of separator thickness beyond which the performance of the lithium ion battery will be impacted due to the limited penetration depth of lithium ions in the cathode materials. Similar results are obtained once the porosity of the separator decreases. The lower the porosity, the fewer routes are available for ionic liquid to pass lithium ions. Fig. 6(a) shows that the performance will be lower if the separator porosity is reduced to 0.15, and the simulation results become unstable after the X mark due to sharp drop in potential. As explained before, this low performance is related to lower cathode utilization (Fig. 6(b)) due to the unavailability of lithium ions. Fig. 6(c) illustrates the lithium ion concentration in the porous cathode region during the final stage of discharge. The concentration gradient across the separator increases with decrease in porosity due to decrease in effective diffusivity. While the low porosity is preferred from mechanical points of view, porosities lower than a threshold value will have significant impact on battery performance.

5.3.2. Effect of Load Current Density and Cathode Thickness

The applied load is a crucial factor in the performance of a battery. Fig. 7(a) shows predicted electric performance of a lithium-ion battery for a 15 microns thick separator and 40 microns thick cathode. The numerical results show that the operating cell potential drops as the load current density increases. This is due to the fact that higher applied current density induces more surface overpotential. However, for moderate increase in the load current density, same maximum specific capacity could be achieved as shown in Fig. 7(a) (see case i_{load} = 1.3 A/m^2 and i_{load} = 2.6 A/m^2). On the other hand, for very high load current density (i_{load}=5.2 A/m^2), the specific capacity is significantly affected due to the lack of lithium ions in the cathode region (not shown). This lack in lithium ion in the cathode region is similar to the case presented in Fig. 5 and 6(c), where the concentration of lithium ions decrease with increase in separator thickness or decrease in separator porosity. Therefore, applied load current density should be restricted to circumvent lithium ion depletion problem, which significantly lowers the specific capacity limit.

We also studied the effect of cathode thickness on the electric performance of a lithium-ion battery to identify the optimum cathode size. In practice, it is desirable to have greater cathode thickness for longer operation of a battery. However, greater thickness increases footprint as well as the weight and volume of the battery. In addition, larger cathode thickness can adversely affect the performance of a lithium-ion battery. Fig. 7(b) shows the electric performance of a lithium ion battery for a load current density of 1.3 A/m^2 and a separator thickness of 15 microns. Numerical results show that for the 20 and 40 μm thick cathodes, same specific capacity limits are obtained. However, for greater cathode thickness (80 μm), the specific capacity decreased considerably due to lithium ion depleted zone (not shown). Therefore, one has to consider the thickness of cathode materials wisely for optimum performance of lithium-ion battery.

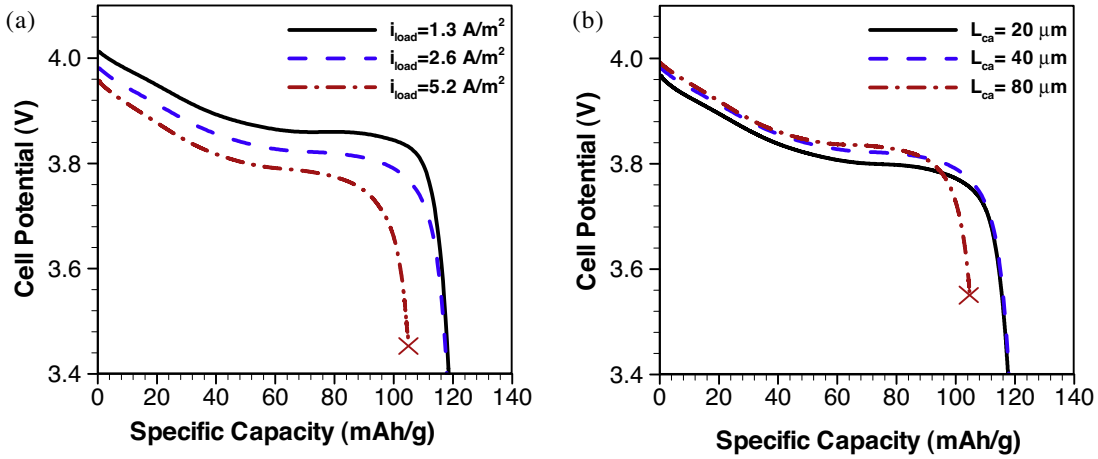

Fig. 7. Dependence of electric performance on (a) applied current density and (b) cathode thickness. All other simulation conditions are the same as in Fig. 3.

6. Conclusions

In this work, a new mathematical model is developed for ternary electrolytes to study next generation ionic liquid based lithium-ion batteries. Lithium ion transport equation and liquid phase electric potential equation are developed considering the strong interactions between the anions and cations of ionic liquid with the lithium ions. To simplify the mathematical model, we took advantage of electro-neutrality and mass conservation of lithium ions in the system. The simplified mathematical model for lithium ion transport is very similar to Nernst-Planck equation, but one has to use apparent diffusivity and mobility to calculate the lithium ion flux. We found that both apparent diffusivity and mobility are a function of Maxwell-Stefan diffusivities and mole fraction of lithium ions. We have used molecular dynamics simulation to estimate the Maxwell-Stefan diffusivities as well as other electrochemical properties in the ternary electrolyte system consisting of mppy+TFSI− doped with Li +TFSI− salt. The developed mathematical model is used to study the performance of a lithium-ion battery, and the predicted electric performance results match very well with experimental findings for moderate value of reaction rate constant. We also studied the effect of separator and cathode thickness on the overall performance of lithium-ion battery. The numerical model suggests that there is an optimum parameter range for thicknesses beyond which the performance of the battery is affected significantly. While very low thickness is prone to mechanical failure, a very thick separator or cathode might cause lithium ion depletion which can lower the cell performance significantly. The model also suggests that the separator porosity should be high enough for enhanced mobility of lithium ions in the system. Furthermore, the applied load current density is an important factor in ionic liquid based lithium-ion batteries.

Acknowledgments

This work was supported in part by the Washington State Joint Center for Aerospace Technology Innovation (JCATI) grant.

References

[1] B. Scrosati, J. Garche, Lithium batteries: Status, prospects and future, Journal of Power Sources 195 (2010) 2419–2430.
[2] T. Nagaura, K. Tozawa, Progressin Batteriesand Solar Cells, Progressin Batteries & Solar, Cells 9 (1990) .
[3] J.R. Dahn, U. Vonsacken, M.W. Juzkow, H. Aljanaby, Rechargeable LINIO2 carbon cells, Journal of the Electrochemical Society 138 (1991) 2207–2211.
[4] D. Guyomard, J.M. Tarascon, Li metal-free rechargeable LiMn2O4/carbon cells - their understanding and optimization, Journal of the Electrochemical Society 139 (1992) 937–948.
[5] S.A. Campbell, C. Bowes, R.S. McMillan, The electrochemical-behavior of tetrahydrofuran and propylene carbonate without added electrolyte, Journal of Electroanalytical Chemistry 284 (1990) 195–204.
[6] D. Guyomard, J.M. Tarascon, High-voltage stable liquid electrolytes for li1 +xmn2o4/carbon rocking-chair lithium batteries, Journal of Power Sources 54 (1995) 92–98.
[7] A. Fernicola, B. Scrosati, H. Ohno, Potentialities of ionic liquids as new electrolyte media in advanced electrochemical devices, Ionics 12 (2006) 95–102.
[8] B. Garcia, S. Lavallee, G. Perron, C. Michot, M. Armand, Room temperature molten salts as lithium battery electrolyte, Electrochimica Acta 49 (2004) 4583–4588.
[9] H. Tokuda, K. Hayamizu, K. Ishii, M. Abu Bin Hasan Susan, M. Watanabe, Physicochemical properties and structures of room temperature ionic liquids. 1. Variation of anionic species, Journal of Physical Chemistry B 108 (2004) 16593–16600.
[10] J. Saint, A.S. Best, A.F. Hollenkamp, J. Kerr, J.H. Shin, M.M. Doeff, Compatibility of LixTiyMn1-yO2 (y=0, 0. 11) electrode materials with pyrrolidinium-based ionic liquid electrolyte systems, Journal of the Electrochemical Society 155 (2008) A172–A180.
[11] H. Sakaebe, H. Matsumoto, N-Methyl-N-propylpiperidinium bis (trifluoromethanesulfonyl) imide (PP 13-TFSI) - novel electrolyte base for Li battery, Electrochemistry Communications 5 (2003) 594–598.
[12] S. Higashi, Y. Kato, K. Takechi, H. Nakamoto, F. Mizuno, H. Nishikoori, H. Iba, T. Asaoka, Evaluation and analysis of Li-air battery using ether-functionalized ionic liquid, Journal of Power Sources 240 (2013) 14–17.
[13] T. Kuboki, T. Okuyama, T. Ohsaki, N. Takami, Lithium-air batteries using hydrophobic room temperature ionic liquid electrolyte, Journal of Power Sources 146 (2005) 766–769.
[14] H. Saruwatari, T. Kuboki, T. Kishi, S. Mikoshiba, N. Takami, Imidazolium ionic liquids containing LiBOB electrolyte for lithium battery, Journal of Power Sources 195 (2010) 1495–1499.
[15] J.S. Newman, Electrochemical systems, Prentice-Hall, Englewood Cliffs, N.J., 1972, 2015.
[16] M. Doyle, Modeling of Galvanostatic Charge and Discharge of the Lithium/Polymer/Insertion Cell, J. Electrochem. Soc Journal of The Electrochemical Society 140 (1993) .
[17] M. Doyle, T.F. Fuller, J. Newman, The importance of the lithium ion transference number in lithium polymer cells, Electrochimica Acta 39 (1994) 2073–2081.
[18] J.T.W. Newman, Porous-electrode theory with battery applications, AIChE J. AIChE Journal 21 (1975) 25–41.
[19] P. Vidts, R.E. De White, Governing equations for transport in porous electrodes, Journal of the Electrochemical Society 144 (1997) 1343.
[20] C.Y. Wang, Micro-Macroscopic Coupled Modeling of Batteries and Fuel Cells, J. Electrochem. Soc. Journal of The Electrochemical Society 145 (1998) .
[21] V.R. Subramanian, J.A. Ritter, R.E. White, Physical and analytical electrochemistry - approximate solutions for galvanostatic discharge of spherical particles - i constant diffusion coefficient, Journal of the Electrochemical Society 148 (2001) E444.
[22] I. Nicotera, C. Oliviero, W.A. Henderson, G.B. Appetecchi, S. Passerini, NMR investigation of ionic liquid-LiX mixtures: Pyrrolidinium cations and TFSI-anions, Journal of Physical Chemistry B 109 (2005) 22814–22819.
[23] A. Deshpande, L. Kariyawasam, P. Dutta, S. Banerjee, Enhancement of lithium ion mobility in ionic liquid electrolytes in presence of additives, Journal of Physical Chemistry C 117 (2013) 25343–25351.
[24] I.B. Sprague, P. Dutta, Modeling of diffuse charge effects in a microfluidic based laminar flow fuel cell, Numerical Heat Transfer Part a-Applications 59 (2011) 1–27.
[25] J. Richter, A. Leuchter, N. Grosser, Digital image holography for diffusion measurements in molten salts and ionic liquids - method and first results, Journal of Molecular Liquids 103 (2003) 359–370.
[26] D.A.G. Bruggeman, Berechnung verschiedener physikalischer Konstanten von hetarogenen Substanzen, Ann. Physik 24 (1935) 636–679.
[27] P.M. Gomadam, J.W. Weidner, R.A. Dougal, R.E. White, Mathematical modeling of lithium-ion and nickel battery systems, Journal of Power Sources 110 (2002) 267–284.
[28] K. Somasundaram, E. Birgersson, A.S. Mujumdar, Model for a bipolar Li-ion battery module: Automated model generation, validation and verification, Applied Mathematics and Computation 219 (2012) 2231–2245.
[29] X. Liu, T.J.H. Vlugt, A. Bardow, Maxwell-Stefan diffusivities in binary mixtures of ionic liquids with dimethyl sulfoxide (DMSO) and H2O, Journal of Physical Chemistry B 115 (2011) 8506–8517.
[30] R. Ditchfield, W.J. Hehre, J.A. Pople, Self-consistent molecular orbital methods. 9. Extended gaussian-type basis for molecular-orbital studies of organic molecules, J. Chem. Phys. 54 (1971) .
[31] W.J. Hehre, R. Ditchfield, J.A. Pople, Self-Consistent Molecular Orbital Methods. 12. Further extensions of Gaussian-type basis sets for use in molecular-orbital studies of organic-molecules, Journal of Chemical Physics 56 (1972) .
[32] S. Plimpton, Fast parallel algorithms for short-range molecular-dynamics, Journal of Computational Physics 117 (1995) 1–19.
[33] E.K. Watkins, W.L. Jorgensen, Perfluoroalkanes: Conformational analysis and liquid-state properties from ab initio and Monte Carlo calculations, Journal of Physical Chemistry A 105 (2001) 4118–4125.
[34] M. Parrinello, A. Rahman, Polymorphic transitions in single-crystals - a new molecular-dynamics method, Journal of Applied Physics 52 (1981) 7182–7190.
[35] S. Nose, M.L. Klein, Constant pressure molecular-dynamics for molecular-systems, Molecular Physics 50 (1983) 1055–1076.
[36] T. Darden, D. York, L. Pedersen, Particle mesh ewald - an n.Log(n) method for ewald sums in large systems, Journal of Chemical Physics 98 (1993) 10089–10092.
[37] J.W. Eastwood, R.W. Hockney, D.N. Lawrence, P3M3DP - THE 3-DIMENSIONAL PERIODIC PARTICLE-PARTICLE-PARTICLE-MESH PROGRAM, Computer Physics Communications 19 (1980) 215–261.
[38] R. Krishna, J.M. van Baten, The darken relation for multicomponent diffusion in liquid mixtures of linear alkanes: An investigation using molecular dynamics (MD) simulations, Industrial & Engineering Chemistry Research 44 (2005) 6939–6947.
[39] K. Yoo, S. Banerjee, P. Dutta, Modeling of volume change phenomena in a Li-air battery, Journal of Power Sources 258 (2014) 340–350.
[40] U. Sahapatsombut, H. Cheng, K. Scott, Modelling the micro-macro homogeneous cycling behaviour of a lithium-air battery, Journal of Power Sources 227 (2013) 243–253.
[41] S.S. Zhang, A review on the separators of liquid electrolyte Li-ion batteries, Journal of Power Sources 164 (2007) 351–364.
[42] D.K. Karthikeyan, G. Sikha, R.E. White, Thermodynamic model development for lithium intercalation electrodes, Journal of Power Sources 185 (2008) 1398–1407.